Proceedings of IGTI 2000
The 45th ASME International Gas Turbine & Aeroengine Technical Congress, Exposition and Users Symposium
May 8-11, 2000 Munich, Germany

2000-GT-405

ANALYSIS AND TESTING OF A MAGNETIC BEARING ENERGY STORAGE FLYWHEEL WITH GAIN-SCHEDULED, MIMO CONTROL

Lawrence A. Hawkins
E-mail: larry@calnetix.com
CalNetix, Inc.
363 Van Ness Way #401
Torrance, CA 90501

Brian T.Murphy **John Kajs**
Center for Electromechanics - University of Texas
Mail Code R7000
Austin, TX 78712

ABSTRACT

The design and initial testing of a five axis magnetic bearing system in an energy storage flywheel is presented. The flywheel is under development at the University of Texas Center for Electromechanics (UT-CEM) for application in a transit bus. The bearing system for the prototype features homopolar permanent magnet bias magnetic bearings. The system has been successfully tested to the maximum design speed of 42,000 rpm. A gain-scheduled, MIMO control algorithm was required to control the system modes affected by rotor gyroscopics. The implementation and basis for this control scheme is discussed. The cross-axis forces produced by this approach are described in terms of circumferential cross-coupled stiffness and damping to explain the effect on system stability. Dynamic test results are discussed relative to the rotordynamic and control system design.

INTRODUCTION

UT-CEM is developing a flywheel energy storage system, conveniently referred to as a flywheel battery (FWB), for use in a power-averaging role in a hybrid electric bus. Energy generated during vehicle braking is converted to mechanical energy by using a motor/generator to drive the FWB. During vehicle acceleration, the motor/generator extracts energy from the FWB, completing the storage/recovery cycle. FWBs are ideal for this application because they have significantly higher power densities and longer life than other types of batteries (Reiner, 1993). The goal of maximizing energy density leads to carbon fiber composites as the material of choice for modern high performance flywheels. These materials can operate safely at surface speeds of 1,000 m/s, as opposed to only 200-300 m/s for metals.

The system under development, shown in Figure 1, is designed to store 2 kWh at 40,000 rpm, and produce 110 kW of continuous power (150 kW peak). The initial testing described here was performed with a 0.8 kWh titanium flywheel rotor having a 9.9 inch outer diameter. This allowed for safe evaluation of the magnetic bearings and motor generator. Now that the bearings and motor generator are fully functional, complete thermal testing is underway. When thermal tests are complete, the titanium rotor will be machined down and composite rings added to bring the outer diameter up to 17.5 inches. This change to the rotor will alter its weight and polar-to-transverse inertia ratio, Ip/It. At that time the control algorithms will require additional refinement for the reconfigured rotor. Hayes, 1998, described the FWB design considerations and low speed testing. The impact of vehicle dynamics on sizing the magnetic bearings for this FWB was described by Murphy, 1996. Hawkins, 1999, described the magnetic bearings and backup bearings for this system in more detail than presented here.

In order to achieve the target operating speed, a gain scheduled MIMO control approach was developed. The cross-axis forces produced by this approach are described in terms of circumferential cross-coupled transfer functions. This discussion describes the influence of the cross-axis terms on the stability of different system modes. Approaches for generating MIMO control algorithms have been described by many authors, including (Matsumura, et al., 1996), (Sivrioglu and Nonami, 1996). These features were applied in a limited way for the current system with titanium flywheel. It is anticipated that future testing of the composite flywheel will require additional sophistication, such as that provided by the more

recent Linear Parameters Varying (LPV) approach (Apkarian and Adams, 1997), (Tsiotras and Knospe, 1997).

NOMENCLATURE

Symbol	Meaning
C	damping matrix or element
F	reaction force
H	impedance function
K	stiffness matrix or element
M	mass matrix
f	force vector
q	physical coordinate vector
ω_n	natural frequency
ω_{spin}	spin frequency
ζ_n	damping ratio
ζ_{ns}	static damping ratio
m	modal coordinate vector
Subscripts	
P	Plant
x,y	Orthogonal radial axes

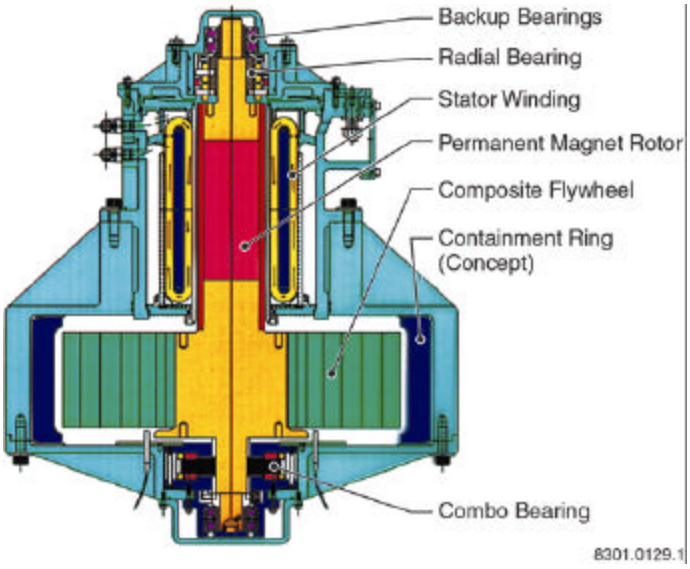

Figure 1. UT-CEM flywheel battery designed for a transit bus.

SYSTEM CHARACTERISTICS

Magnetic Bearing

The magnetic bearings are homopolar, permanent magnet bias bearings. The combo bearing in Figure 1 is a three-axis combination radial/thrust bearing. This design uses a single radially polarized permanent magnet ring to provide bias flux for the both the radial and axial flux paths. Three separate pairs of control coils allow individual control of each axis. The radial bearing (Brg 2) is a two-axis radial bearing. The basic operation of this bearing was described by Meeks (1990). Some characteristics of the magnetic bearings are given in Table 1.

Table 1. Magnetic Bearing Characteristics.

Bearing	Combo Bearing (Radial)	Radial Bearing	Combo Bearing (Axial)
Bearing Reference Name	Brg 1	Brg 2	Thrust
Channel Names	1,2	3,4	5
Coordinate Names	*x1,y1*	*x2,y2*	*z*
Peak Load Capacity, N (lbf)	1115 (250)	670 (150)	2230 (500)
Force Constant, N/A (lbf/A)	156 (35)	94 (21)	303 (68)
Negative Stiffness, N/mm (lbf/in)	1751 (10,000)	963 (5500)	3502 (20,000)
Air Gap, mm (in)	0.508 (.020)	0.508 (.020)	0.508 (.020)
Backup Brg Clearance, mm (in)	0.254 (.010)	0.254 (.010)	0.254 (.010)

Rotordynamic Model

The rotordynamic structural model is shown in Figure 2. The actuator and sensor locations and the first free/free, zero-speed bending mode are superimposed on the plot. Notice that the sensor and actuator modal displacements are lower at Brg 1 compared to Brg 2 in the first bending mode. The first four bending modes are included in the system analysis. The frequencies of those modes at zero speed are: 745 hz, 1425 hz, 1990 hz, and 3590 hz.

The rotordynamic equation of motion for the plant, which is in general a coupled, flexible rotor/casing system with conventional bearings, is:

$$[M]\{\ddot{q}\}+[C]\{\dot{q}\}+[K]\{q\}=\{f\} \qquad \textbf{(1)}$$

The passive negative stiffness of the magnetic bearing is included in the bearing stiffness matrix, K. The terms representing gyroscopic effects are part of the rotor partition of the damping matrix, C.

For the flywheel, each rotor bending mode was given a static internal damping ratio, ζ_{ns}=0.5%. This is a reasonable value for a rotor with sleeves if no modal test data is available. The internal damping for rotor modes is reduced as speed increases by:

$$\zeta_n = \zeta_{ns}\left(\frac{\omega_n - \omega_{spin}}{\omega_n}\right) \qquad (2)$$

The basis for this circular whirl approximation can be derived from the discussion of internal rotor damping by Childs (1993).

For system analysis with magnetic bearings, the plant represented by Eqn. (1) is transformed to modal coordinates and converted to state space form:

$$\{\dot{m}_P\} = [A_P]\{m_P\} + [B_P]\{f\}$$
$$\{q\} = [C_P]\{m_P\} + [D_P]\{f\} \qquad \textbf{(3)}$$

Partitions of the characteristic matrix A_P contain the modal stiffness and damping matrices. The input and output matrices B_P and C_P contain mass normalized eigenvectors for modes selected for the system analysis. Some authors include the passive negative stiffness as part of the feed forward matrix D_P instead of as a bearing stiffness in K. These equations have been presented in detail by several authors; one recent example is Antkowiak (1997).

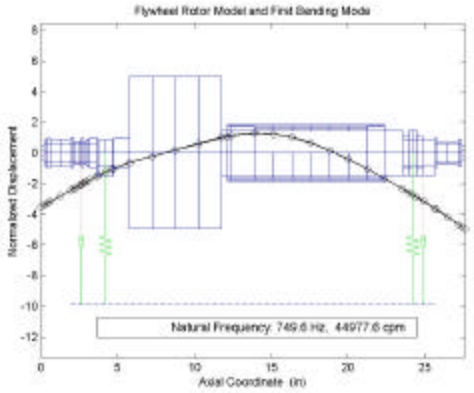

Figure 2. Rotordynamic Structural Model with First Bending Mode.

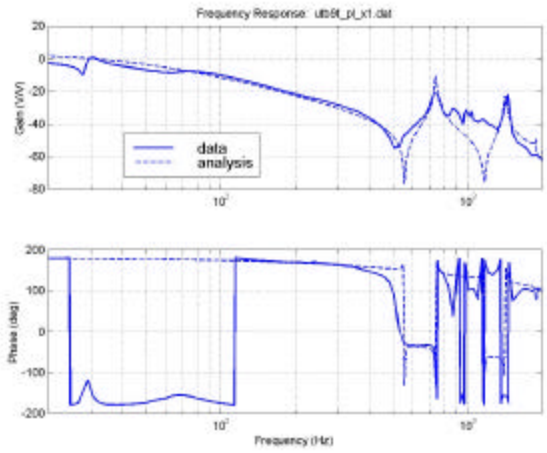

Figure 3. Predicted vs. Measured Actuator/ Plant/Sensor Bode Plot (x1 axis).

Predicted and measured plant bode plots are shown in Figure 3 for zero speed. Both curves include the bearing and sensor dynamics because the plant must be measured in the installed system by taking the transfer function between the position sensor and the amplifier current monitor. The phase roll-off seen in Figure 3 beginning around 100 hz is due to the low pass filter (bandwidth of 3.4 kHz) in the position sensor demodulation electronics. The weak mode at about 30 hz in the measured transfer function is the rigid body mode of the system on the elastomeric housing supports. Due to its limited influence on the control of the rotor, the housing was not included as part of the plant model for this stage of the FWB analysis. Although the coherence of the measured result is poor above 800 hz, the first two bending modes at 750 and 1425 hz are apparent and consistent with the model.

System Analysis

The initial magnetic bearing transfer function for Brg 1 (*x1* and *y1*) is given in Figure 4. This is the analytical force/displacement transfer function, which includes the dynamics of the position sensor, compensator, amplifier, and actuator. The transfer function for Brg 2 is similar. For linear response and eigenvalues analysis, the magnetic bearing transfer functions are converted to state space form and coupled to the plant model of Equation 3. Figure 5 is a plot of all system natural frequencies below 1000 hz that have damping ratios (ξ) less than 0.25. Well damped modes were left out because the large number of such modes in the system make this type of plot difficult to interpret. The strong gyroscopic influence is responsible for the rise of the second rotor rigid body mode with speed as well as the spread of the forward and backward bending modes (see Figure 5).

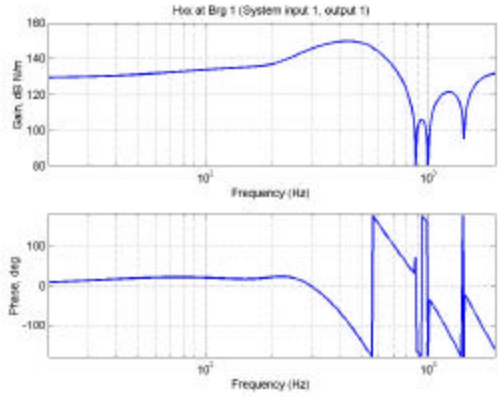

Figure 4. Single Speed SISO Mag Bearing Transfer Function, includes Sensor/ Compensator/Amplifier/Actuator

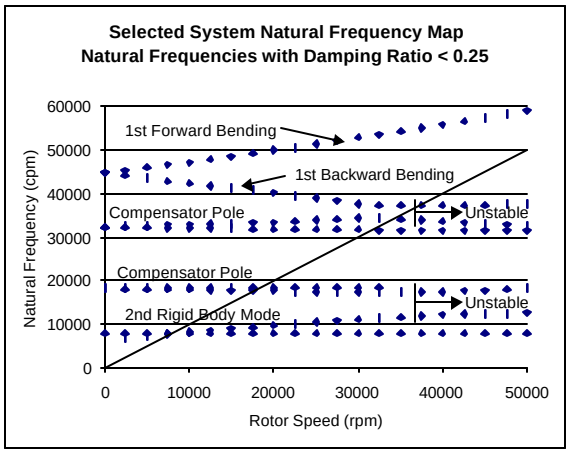

Figure 5. Selected System Natural Frequencies, ζ<0.25 with Speed Independent SISO Controller.

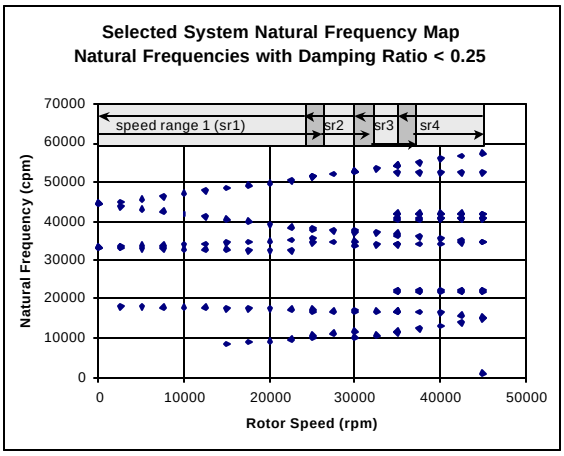

Figure 6. Selected System Natural Frequencies, ζ<0.25Gain Scheduled MIMO Controller (speed ranges shown at top).

CONTROL SYSTEM DEVELOPMENT

Speed Independent, SISO Control Approach

The magnetic bearing system was originally designed and built by Avcon, a company that ceased operation just as the flywheel was initially assembled. Due to limited processing power of the DSP in the controller supplied with the system, the original control hardware allowed only SISO compensation with a maximum of six biquad filters per axis at a 10 kHz sample rate. No speed input was provided, thus a successful compensation would have to control all modes of the system from rest to 42,000 rpm. This task is readily achievable for some types of rotors, but not practical for a rotor with substantial gyroscopic effects such as this FWB. Stability of the rigid body conical mode and/or the backward first bending mode was marginal at all speeds above 30,000 rpm. The highest speed achieved with the SISO single speed controller was 37,000 rpm.

The SISO transfer function was shown in Figure 4. The control algorithm provides direct phase lead for the second rigid body mode. The compensation rolls off sharply above the rigid body mode, again providing phase lead for the backward and forward components of the first bending mode. At higher rotor spin speeds, the forward bending mode exits the positive phase lead region near 900 hz. The mode is still stable due to the low gain of the transfer function at those frequencies. This strategy has a limit in that at higher speeds, the frequencies of the forward rigid body mode and the first backward bending mode become close enough that the phase cannot be transitioned quickly enough between the modes. That limit was reached at 37,000 rpm for this rotor and the original control hardware.

Gain Scheduled, MIMO Control Approach

Hardware Development

In order to bring the machine to full speed operation, CalNetix developed a new stand-alone control module based on the Texas Instruments TMS 320C6201 (C6x) digital signal processor (DSP). This control module provided a factor of 5 to 10 increase in processing speed, program and data memory. Whereas the previous control module had to be programmed in assembly and used 80 µs (80% of available processing time at a 10 kHz sample rate) to execute the desired set of transfer functions for the flywheel (a 12 state compensator for each radial axis, 4 states for the axial), the new control module could execute the same set of transfer functions in about 15 µs with a control program written in C. Since a 10 kHz sample rate is suitable for most magnetic bearing supported turbomachinery, the new control hardware comfortably allows at least five times as many instructions as the previous hardware. The new control hardware also allowed the easy incorporation of a speed/phase detection scheme. Thus previously unavailable MIMO and gain scheduled control schemes could now be used.

Gain Scheduling Implementation

As an initial implementation of gain scheduled control, the control program was structured to access up to four independent sets of control parameters (filter coefficients and gains). Each set of control parameters is applied in a different rotor spin speed range. The speed ranges overlap so that the selected set of control parameters is prevented from toggling back and forth near a transition speed. The speed ranges for the FWB are indicated on the natural frequency map of Figure 6. When the spin speed moves into a new speed range, the pointer to the coefficient table in memory is moved to the start of the next coefficient table. This feature allows the use of a transfer function that is optimized more closely to the plant requirements within a given speed range than can be accomplished with a single control structure. The choice of four speed ranges was made simply to address the (now) well-known needs of the titanium FWB. The only hard limit to the number of speed ranges imposed by the control module is the amount of data memory used, which is about 1 kB per speed range with the structure now in use.

Since robust operation had been achieved to 30,000 rpm with a single set of control parameters, the initial implementation of gain scheduling focused on simple modifications to this compensation. Parameters for the first speed range were modified to provide more damping at the rigid body critical speeds. The resulting damping ratios were approximately: 0.38 and 0.32 respectively. The control parameters for the three higher speed ranges successively track the second forward rigid body mode and first backward bending mode, at the expense of reduced damping at 50-150 hz since the critical speeds have already been traversed.

Circumferential Cross-Coupling Implementation

In order to further improve the damping ratios of the troublesome modes, a simple MIMO control feature was also added to the control program. For the test results presented in this paper, the MIMO feature was used only for the fourth speed range, but it can just as easily be used in any or all speed ranges as desired. As with the SISO controller, the magnetic bearing control commands are calculated from a series of cascaded biquad filters that produce the desired transfer functions. Five direct axis transfer functions are used to represent the normal SISO control for a five-axis system. SISO implies that each axis is controlled independently of the others. In the MIMO implementation employed here, up to four additional transfer functions are provided which can be used with independently selectable input and output axes. The intended use for this feature is for circumferential (*x*,*y*) cross-coupling; however, the selection of input and output channels is general, allowing this feature to be used in other ways.

DISCUSSION OF CIRCUMFERENTIAL CROSS-COUPLING

The application of circumferential cross-coupling for stability improvement is well suited to the flywheel because the forward and backward modes are well spaced in the frequency spectrum. The forces that are applied by the cross-coupled terms can be understood in the following way. Consider a radial bearing to have two orthogonal axes, *x* and *y*. In a SISO controlled magnetic bearing, the bearing reaction force, *F*, along a given axis is due to motion only along that same axis. That is, if the rotor moves in the *x* axis direction, this produces a bearing force along only the *x* axis. This is illustrated in Eqn. (4):

$$\begin{Bmatrix} F_x \\ F_y \end{Bmatrix} = -\begin{bmatrix} H_{xx} & 0 \\ 0 & H_{yy} \end{bmatrix} \begin{Bmatrix} x \\ y \end{Bmatrix} \qquad (4)$$

For magnetic bearings, the H_{ij} are called transfer functions, and are generally functions of frequency. The frequency dependence in a magnetic bearing is defined by the control compensation in conjunction with the dynamic characteristics of other parts of the system such as the position sensor, power amplifier, and magnetic actuator. In a MIMO controlled magnetic bearing, the off-diagonal terms can be nonzero. This is called *circumferential* cross-coupling since the *x* and *y* axes within one radial bearing are being coupled. In this case, motion in one axis, say *x*, produces forces in *both* the *x* and *y* axes. This is illustrated in Eqn. (5):

$$\begin{Bmatrix} F_x \\ F_y \end{Bmatrix} = -\begin{bmatrix} H_{xx} & H_{xy} \\ H_{yx} & H_{yy} \end{bmatrix} \begin{Bmatrix} x \\ y \end{Bmatrix} \qquad (5)$$

The H_{xy} and H_{yx} are the circumferential cross-coupling transfer functions. Another potentially attractive type of cross-coupling would be between the *x* axes (or *y* axes) of two radial bearings working in tandem to support a rotor.

Insight into the impact of circumferential cross-coupling on rotordynamic behavior can be gained from the study of hydrodynamic bearings. For modeling purposes, the *H* functions are usually expressed as follows:

$$H_{ij}(\omega) = K_{ij} + i\omega C_{ij} \quad . \quad \text{subscripts } i=x,y, \;\; j=x,y \qquad (5)$$

K_{xx} is a stiffness value. Forces attributed to this parameter are always conservative. C_{xx} is a damping value so forces attributed to it are nonconservative. This situation is reversed for cross-coupling parameters. The special case of $K_{xy} = -K_{yx}$ produces a nonconservative force that is always orthogonal to the rotor displacement vector. So it is either stabilizing or destabilizing depending on whether the rotor's orbit path is forward or backward relative to the direction of spin. Since the forces are nonconservative, they exert much the same influence as regular damping, except that it now also depends on the direction of whirl. The special case of $C_{xy} = -C_{yx}$ produces a conservative force that is always orthogonal to a vector tangent to the rotor orbit path. So it can actually behave much like a stiffness parameter, working to recenter the rotor. It is either centering or decentering depending on whether the rotor's orbit path is forward or backward relative to the direction of spin.

The force vector diagrams in Figure 7 illustrate the action of the cross-coupled terms. In the figure, the direction of spin is counterclockwise, and a forward orbit is then also counterclockwise. In each individual term like K_{xy}, the first subscript is the direction of the force (magnetic bearing output) due to motion in the axis of the second subscript (magnetic bearing input). In the stiffness force diagram, the force shown will drive (destabilize) a forward mode, and retard (stabilize) a backward mode. In the damping force diagram, the force shown will tend to center a forward mode, and decenter a backward mode. The cause and effect of the different combinations are

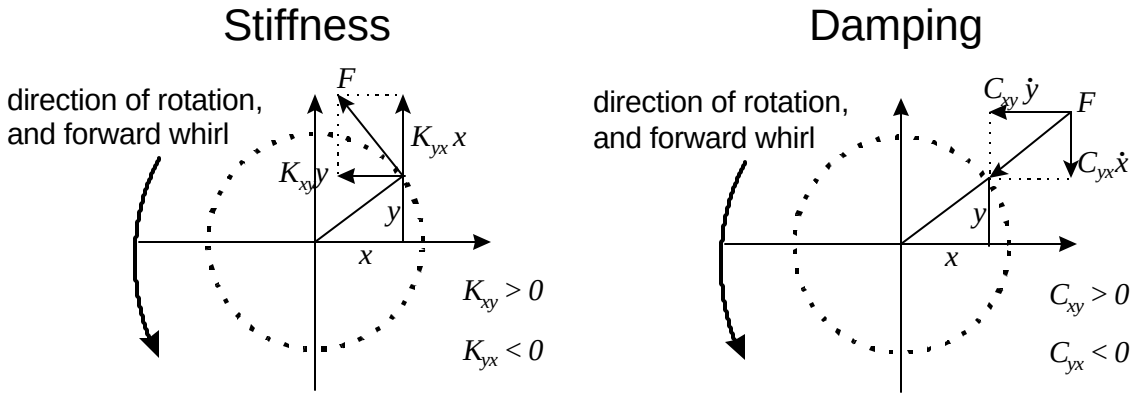

Figure 7. Force vector diagram for cross-coupling functions. Forces shown correspond to a forward whirling orbit.

summarized in Table 2. The opposing effect of cross-coupled forces on forward and backward modes makes stabilizing circumferential cross-coupling best suited to gyroscopic rotors (like flywheels) that have wide spacing between forward and backward modes in the frequency spectrum.

Table 2. Summary of Cause and Effect of Cross-Coupled Transfer Function Terms.

Terms	Description	Effect
$K_{xy} > 0$ $K_{yx} = -K_{xy}$	Cross-coupled stiffness	Destabilizes forward modes Stabilizes backward modes
$K_{xy} < 0$ $K_{yx} = -K_{xy}$	Cross-coupled stiffness	Stabilizes forward modes Destabilizes backward modes
$C_{xy} > 0$ $C_{yx} = -C_{xy}$	Cross-coupled damping	Stiffens forward modes De-stiffens backward modes
$C_{xy} < 0$ $C_{yx} = -C_{xy}$	Cross-coupled damping	De-stiffens forward modes Stiffens backward modes

Two of the four cross-coupled transfer functions used for the FWB are given in Figures 8 - 9. Both of these transfer functions include the dynamics of the position sensor, amplifier and magnetic actuator, and a Pade approximation of the calculation phase delay. These elements are part of the impedance or magnetic bearing transfer function. Figure 8 is the transfer function between input 2 and output 1 (H_{xy} for Brg 1). The transfer function between input 1 and output 2 (H_{yx} for Brg 1) is the same except that the gain term carries the opposite sign, making the phase different by 180°. Figure 8(b) shows the same transfer function, converted to equivalent cross-coupled stiffness (K_{xy}) and cross-coupled damping (C_{xy}) coefficients per Equation 5. Together with the opposite signed K_{yx}, this transfer function produces a stabilizing force on forward modes (and a destabilizing force on backward modes) with frequencies up to abo ut 300 hz (21,000 cpm). For modes above 300 Hz, the force is destabilizing for forward modes and stabilizing for backward modes.

Figure 9 is the transfer function between input 4 and output 3 (H_{xy} for Brg 2). H_{yx} for Brg 2 is the same as H_{xy} except that again the gain term carries the opposite sign, making the phase different by 180°. The cross-coupled transfer function applied at Brg 2 is designed specifically to provide a stabilizing force for the first backward bending mode of the rotor which is near 30,000 cpm when the rotor speed is in the range of 35,000 to 42,000 rpm.

DYNAMIC TEST DATA

Figures 10 - 12 show dynamic data collected from a full-speed rundown of the machine. During rundown, the motor generator is used to decelerate the rotor from 42,000 rpm to rest in approximately 90 seconds. Figure 10 is a plot of synchronous displacements taken from the magnetic bearing position sensors during the spin-down. There is a spike at about 1,500 rpm on all sensors due to the traverse of the housing support mode. A significant displacement at Brg 2 occurred near the expected traverse of the second rotor rigid body mode at 8,000 rpm. There is also significant displacement at Brg 1, near the traverse of a lightly damped system mode at 15,000 - 18,000 rpm. This mode is closely related to the second rigid body mode and the compensator pole that provides phase lead for the mode. These response peaks agree well with the mode locations in Figure 6. The synchronous displacements also begin to rise again between 30,000 and 42,000 rpm as the net direct stiffness of the bearing falls. Figure 11 is a plot of synchronous coil current for each bearing. The magnetic bearing control current diminishes between 30,000 and 42,000 rpm in tandem with the rise in rotor displacements. This is because the stiffness (gain) of the bearing transfer function drops significantly in this frequency range (see Figure 4). Note that the current curves exhibit steps at 24,000, 30,000, and 35,000 rpm. These are the switching points for the gain scheduling when the rotor is spinning down in speed.

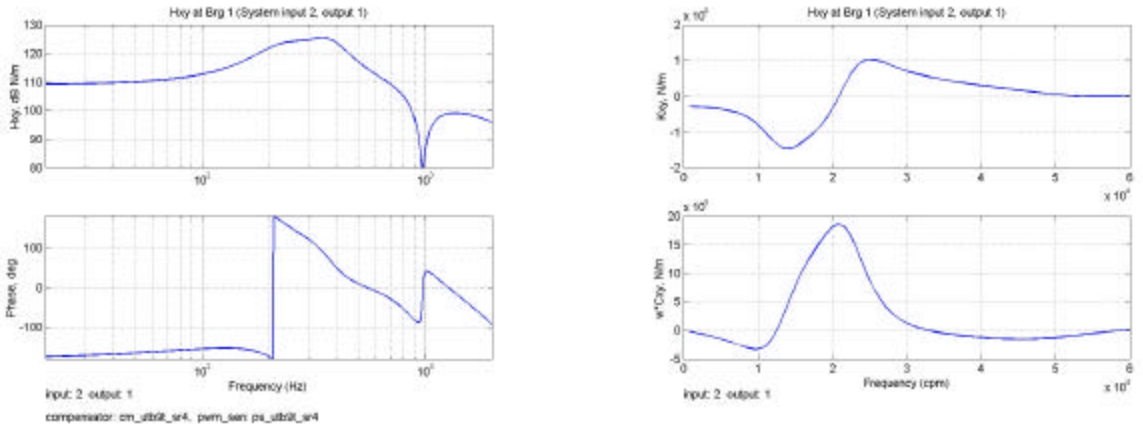

Figure 8. Hxy at Brg 1: (a) gain and phase, (b) Kxy and wCxy.

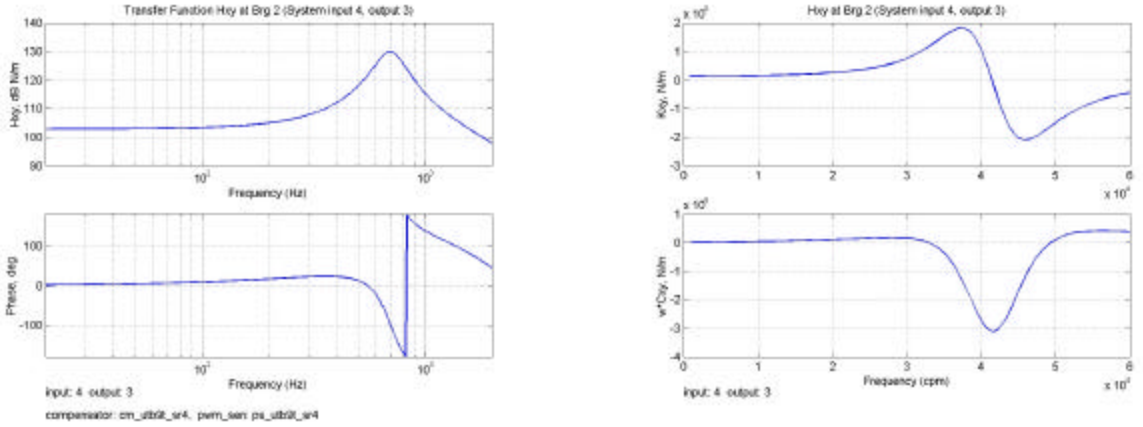

Figure 9. Hxy at Brg 2: (a) gain and phase, (b) Kxy and wCxy.

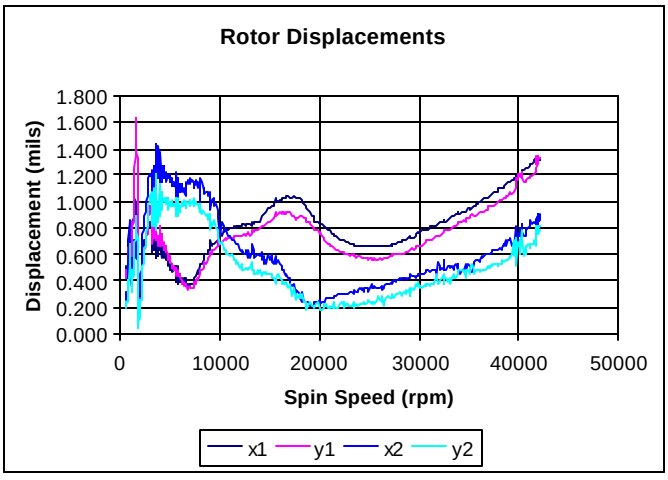

Figure 10. Synchronous Displacements during Spin Down from Full Speed.

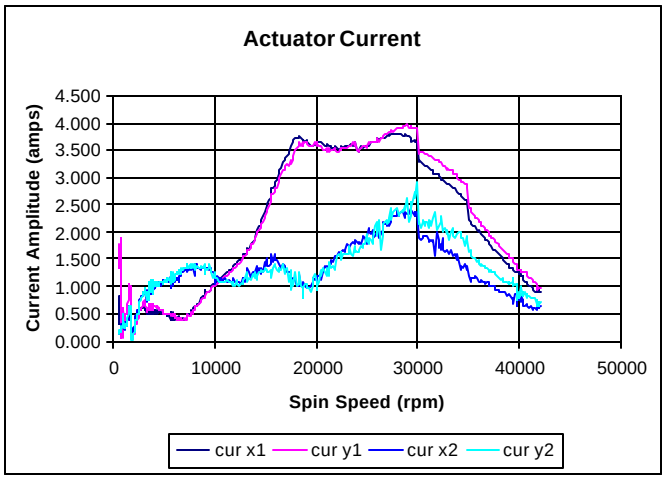

Figure 11. Synchronous Coil Current during Spin Down from Full Speed.

A waterfall plot for the *x*1 axis (Brg 1, input 1) position sensor is shown in Figure 12. The waterfall shows the frequency spectrum for a large number of spin speeds during the spin down from 42,000 rpm to 5,000 rpm. Two decades of the amplitude spectrum are shown, and the clearly dominant signal is the rotor synchronous displacement (700 hz at 42,000 rpm). The forward and backward bending modes are intermittently visible; they are at about 560 hz and 920 hz at 42,000 rpm, converging to 750 hz at low speed. The mode visible near 250 hz (42,000 rpm spin speed) is the second rigid body mode. This mode drops to about 150 hz at rest. The locations of these modes are in agreement with the predicted natural frequencies in Figure 6. The speed independent response at 720 hz is noise.

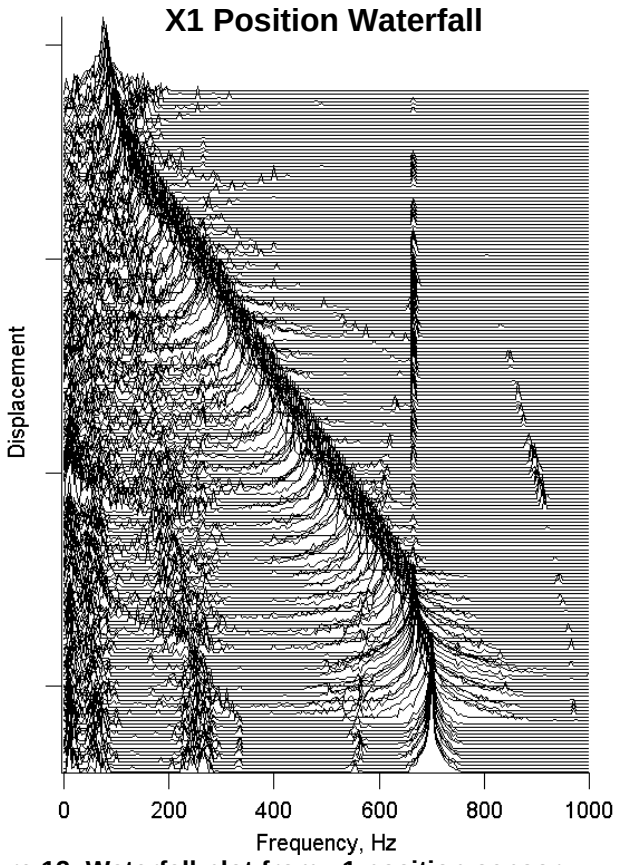

Figure 12. Waterfall plot from x1 position sensor during spindown from 42,000 rpm to 5,000 rpm.

CONCLUSION

System analysis and development of a magnetic bearing system for an energy storage flywheel was described. Development and implementation of a gain-scheduled, MIMO digital control scheme was discussed. The vector forces produced by the MIMO control, which was implemented as circumferential cross-coupling, were also described in terms of coefficients used in conventional bearing analysis. Dynamic test data from full speed testing of the system showed good performance from the bearings and control system. Good agreement was found between the system analysis and test data.

REFERENCES

Ankowiak, B.M., Nelson, F.C., 1997, "Rotordynamic Modeling of An Actively Controlled Magnetic Bearing Gas Turbine Engine", ASME 97-GT-13, 1997 IGTI Turbo-Expo, Orlando.

Apkarian, P. and Adams, R.J., 1997, "Advanced Gain-Scheduling Techniques for Uncertain Systems," IEEE Trans. on Control Systems Technology, Vol. 6, no. 1, pp. 21-32.

Childs, D.W., 1993, "Turbomachinery Rotordynamics", J. Wiley, New York, p. 25.

Hawkins, L.A., Murphy, B.T., Kajs, J.P., 1999, "Application of Permanent Magnet Bias Magnetic Bearings to an Energy Storage Flywheel", 5th Symposium on Magnetic Suspension Technology, Santa Barbara.

Hayes, R.J., Kajs, J.P., Thompson, R.C., Beno, J.H., 1998, "Design and Testing of a Flywheel Battery for a Transit Bus", SAE 1999-01-1159.

Matsumura,F., Namerikawa, T., Hagiwara, K., and Fujita, M, 1996, "Application of Gain Scheduled H∞ Robust Controllers to a Magnetic Bearing," IEEE Transactions on Control Systems Technology, Vol. 4, no. 5, pp. 484-492.

Meeks, C.R., DiRusso, E., Brown, G.V. , 1990, "Development of a Compact, Light Weight Magnetic Bearing", AIAA/SAE/ SME/ASEE 26th Joint Propulsion Conference, Orlando.

Murphy, B.T., Beno, J.H., Bresie, D.A. , 1997, "Bearing Loads in a Vehicular Flywheel Battery", PR-224, SAE Int. Congress and Exp., Detroit.

Reiner, G. , 1993, "Experiences with the Magnetodynamic (Flywheel) storage System (MDS) in Diesel Electric and Trolley Busses in Public Transport Service," Pres. at Flywheel Energy Storage Technology Workshop, Oak Ridge Tenn.

Sivrioglu, S. and Nonami, K., 1996, "LMI Approach to Gain Scheduled H∞ Control Beyond PID Control for Gyroscopic Rotor-Magnetic Bearing Systems," Proc. 35th Conf. On Decision and Control, pp. 3694-3699, Kobe, Japan.

Sivrioglu, S. and Nonami, K., 1998, "An Experimental Evaluation of Robust Gain Scheduled Controllers for AMB System with Gyroscopic Rotor", Proc. of the 6th Int. Symp. On Magnetic Bearings, p. 352-361, Cambridge, MA.

Tsiotras, P. and Knospe, C, "Reducing Conservatism for Gain-Scheduled H∞ Controllers for AMB's", Proc. of MAG'97, p. 290-299, Alexandria, VA.